Moist Stability of a Baroclinic Zonal Flow with Conditionally Unstable Stratification

BIN WANG

Geophysical Fluid Dynamics Program, Princeton University, Princeton, NJ 08542

ALBERT BARCILON

Geophysical Fluid Dynamics Institute and Department of Meteorology, Florida State University, Tallahassee, FL 32306

(Manuscript received 8 July 1985, in final form 8 November 1985)

ABSTRACT

The moist stability of a midlatitude zonal flow with a conditionally unstable layer in the presence of an Ekman layer is investigated. The vertical velocity employed in a simplified Kuo's parameterization is sustained by baroclinic wave forcing, diabatic heating and Ekman pumping. A general dispersion relation and eigenfunction are derived analytically for a class of flows with various vertical heating profiles.

The moist unstable mode may be regarded as a baroclinic wave modified by the bulk effect of the convective heating, for which the fundamental dependences of the baroclinic growth rate on the Burger number and vertical shear remain qualitatively valid. Waves longer than the Rossby radius of deformation are not appreciably affected, while the shorter waves are significantly destablized by the convective heating. The growth rates and wavelengths of the most unstable modes are nonlinear functions of the averaged specific humidity of the moist layer, and there is an optimum specific humidity that minimizes the preferred wavelength, this value being proportional to the static stability for a representative heating profile. The quasi-geostrophic constraints and baroclinity appear to be decisive factors that suppress short waves and lead to a finite preferred wavelength.

The destabilizing effect of the convective heating is considerably enhanced by the reduction of the static stability. Among the other influential parameters that affect the growth rate, relatively lower cloud top and a deep moist layer have a profound effect on the stability. Because of the cooperative interactions between favorable factors, the simultaneous occurrence of several of the mechanisms listed above may produce explosive-like growth. The relatively shallow convection and the Ekman layer will slow down the wave propagation speed.

1. Introduction

The theory of barcolinic instability established by Charney (1947) and Eady (1949) has been the cornerstone of the quasi-geostrophic theory. It provided a reasonable explanation of the generation of midlatitude synoptic disturbances when the available potential energy of the westerlies is the dominant energy source. However, the theory excluded diabatic heating, which plays an important role in the development of the moist midlatitude disturbances, as indicated by a number of diagnostic studies (e.g., Tracton, 1973; Smith et al., 1984).

Cumulus convection often occurs in association with the development of midlatitude cyclones in an atmosphere with a conditionally unstable layer. Particularly, the explosive deepening was found to take place once the cumulus convection becomes organized in areas adjacent to the storm center (Bosart, 1981; Gyakum, 1983b). The extratropical cyclones exhibit an asymmetric pattern of convection with respect to the vortex axis, the strongest convective area being found north and east of the vortex in the region of the strong surface wind (Bosart, 1981). These observations have led to the belief that the importance of cumulus convection cannot be ruled out. The concept of CISK (conditional instability of the Second Kind), which has been instrumental in understanding the dynamics of hurricanes and tropical disturbances, may also be applicable to midlatitude disturbances (Rasmussen, 1979).

So far, there are few analytical studies that incorporate the effect of convective latent heating into the quasi-geostrophic baroclinic theory. Gambo (1976) considered a prototype of this problem and showed that the characteristics of the unstable disturbances depend upon a parameter λ, which loosely represents the ratio of the vertical velocity due to the frictional convergence in the boundary layer to that of the baroclinic wave. His approximate solutions were limited by the assumptions of $\lambda \ll 1$ or $\lambda \gg 1$ and the uniform vertical heating distribution. Mak (1982) considered an Eady model with a CISK parameterization and showed that, as the heating intensity parameter is increased, the growth rate and the phase speed of the most unstable wave significantly increase, while its wavelength significantly decreases. In his formulation, the vertical velocity used in the parameterization of the diabatic heating was only related to the rotational wind field through the omega-equation; this approximation was based on the perception that it leads to a wave selection.

However, since the vertical velocity at the top of the low-level convergence layer is partly driven by the latent heat release, the consequences of this conceptual assumption on the wave selection mechanism and wave characteristics ought to be studied. Sardie and Warner (1983) used a three-layer, quasi-geostrophic model in which latent heating is parameterized for both stable precipitation and convective precipitation associated with CISK. They found that CISK alone is not sufficient for the genesis of polar lows, while baroclinic instability with CISK appears to be essential for the genesis of Atlantic polar lows. Since the solution with CISK was shown to be sensitive to the vertical resolution of the model (Chang and Williams, 1974; Anthes et al., 1983) some of Sardie and Warner's results may suffer from the poor vertical resolution of their model; for example, the wave selection undergoes large changes when the heating in the lower layer changes by small amounts. In their calculation for several case studies of polar lows, Sardie and Warner (1983) showed that the incorporation of the CISK mechanism increases the growth rate, on average, by only some 40% (their Table 3), while Mak (1982) concluded that the maximum growth rate can be as large as five times that of the dry model. There is also some disagreement on the wavelength of the most unstable mode.

A central question can be raised: How important is convective heating during explosive cyclogenesis? The answer to this question is tied to the following points which require clarification: What is the dynamical nature of the unstable wave in a baroclinic zonal flow in the presence of CISK? How do the instability characteristics change as we consider different vertical-heating profiles and basic states characterized by different properties? Is there any possible cooperation among the various influential factors that results in extraordinarily large growth? We propose to seek answers to these questions.

2. Model formulation

We consider a linear, y-independent, quasi-geostrophic perturbation about a zonally averaged basic state, which is assumed to be a function of pressure only, i.e., $U = U(p)$ and $\sigma \equiv -\alpha\partial \ln\theta/\partial p = \sigma(p)$, where U is the zonal velocity, σ is the static stability, and α and θ are the specific volume and potential temperature, respectively. The perturbation quasi-geostrophic vorticity and thermodynamic equations, when expressed in an f-plane in the p-coordinate, can be written as

$$\left(\frac{\partial}{\partial t} + U\frac{\partial}{\partial x}\right)\frac{\partial^2\phi}{\partial x^2} = f_0\frac{\partial\omega}{\partial p}, \tag{2.1a}$$

$$\left(\frac{\partial}{\partial t} + U\frac{\partial}{\partial x}\right)\frac{\partial\phi}{\partial p} - \frac{dU}{dp}\frac{\partial\phi}{\partial x} + \frac{\sigma}{f_0}\omega = -\frac{R}{f_0C_pp}\dot{H}, \tag{2.1b}$$

where ϕ represents the perturbation geostrophic streamfunction, $\dot{H}$ denotes the diabatic heating rate per unit mass, $\omega \equiv dp/dt$ is the vertical p-velocity, R the gas constant, C_p the specific heat at constant pressure, and f_0 the constant Coriolis parameter. The justification for the f-plane geometry will become apparent in what follows.

Based upon observations of rapidly deepening cyclones (Gyakum, 1983a), we assume that the model atmosphere is gravitationally stable for the large-scale motion but unstable for the convective-scale motion, i.e., there exists a conditionally unstable layer in which cumulus clouds are present. We further assume that condensation occurs primarily through cumulus convection and neglect other diabatic heatings. As mentioned in previous section, the observations suggest that baroclinic waves organize cumulus convection, and their rapid developments are often accompanied by noticeable cumulus latent heat release. We presume that there exist dynamic and thermodynamic interactions between midlatitude baroclinic wave and cumulus scale motions in the presence of conditionally unstable layers. The baroclinic waves are heated by cumulus convection which is, in turn, controlled by the synoptic scale moisture convergence. A simple parameterization of this scale interaction can be based upon Kuo's (1965, 1974) scheme, where the latent heat release due to deep convection, is parameterized by

$$\dot{H} = \frac{g(1-b)L_cM_t[T_c(p) - T(p)]\theta/T}{\int_{p_t}^{p_b}(T_c - T)dp} \tag{2.2}$$

where T and θ are the environmental temperature and potential temperature, respectively; T_c is the temperature within the cloud; p_b and p_t are the pressures at cloud base and top; L_c is the latent heat of condensation; g is gravity; M_t denotes the rate of moisture convergence from the surface to the cloud top, including horizontal convergence of specific humidity and evaporation of water from the lower boundary; b is the fraction of M_t stored in the air to increase the specific humidity of the environment. For mathematical tractability, we shall further assume that 1) the moisture convergence is primarily confined to a lower moist layer, where the specific humidity is a constant $\bar{q}$, and 2) the feedback by which the wave field affects the heating distribution can be neglected, and the vertical heating profile is then specified empirically by $\eta(p)$. With these two additional assumptions, (2.2) becomes

$$\dot{H} = -\frac{\tilde{\alpha}L_c}{P_0}(\bar{q}\omega(p_m) - gE)\eta(p), \tag{2.3a}$$

where p_m is the pressure at the top of the moist convergence layer, P_0 the surface pressure, E is the surface evaporation rate, $\eta(p)$ must satisfy

$$\frac{1}{P_0}\int_0^{P_0}\eta(p)dp = 1,$$

and

$$\tilde{\alpha} = (1 - b) \cdot \frac{\int_{p_t}^{p_b} (T_c - T) \frac{\theta}{T} dp}{\int_{p_t}^{p_b} (T_c - T) dp} \tag{2.3b}$$

is a nondimensional coefficient, proportional to the ratio of convective precipitation to the total moisture convergence into the cumulus cloud ensemble. When the background relative humidity is large, b is assumed to be zero. We shall take $\tilde{\alpha} \approx 1$ for convenience. Equation (2.3) relates the heating coefficient directly to the moisture content $\bar{q}$, which can be viewed as a measure of the potential moist energy of the basic zonal flow and of the heating intensity. In our parameterization, $\dot{H}$ does not vanish when $\omega(p_m) > 0$, i.e., there is cooling in the presence of downward motion.

A continuously stratified model will be used, partly because the CISK solution is sensitive to the vertical resolution of the model, and partly because a continuous model contains more of the relevant physics in the CISK parameterization. The motion is confined between two horizontal boundaries found at $p = p_u$ and $p = p_e$, where p_u may be viewed as the pressure at tropopause or at infinite height ($p_u = 0$), and p_e represents the pressure at the top of the lower Ekman layer. A schematic representation of the model is shown in Fig. 1. The vertical velocity is assumed to vanish at the upper boundary and to match the Ekman pumping velocity at the lower boundary, i.e.,

$$\omega = 0, \quad \text{at} \quad p = p_u, \tag{2.4a}$$

$$\omega = -\rho_0 g \left(\frac{K}{2f_0}\right)^{1/2} \frac{\partial^2 \phi}{\partial x^2}, \quad \text{at} \quad p = p_e, \tag{2.4b}$$

where K represents the vertical eddy viscosity coefficient and ρ_0 represents the density at p_e.

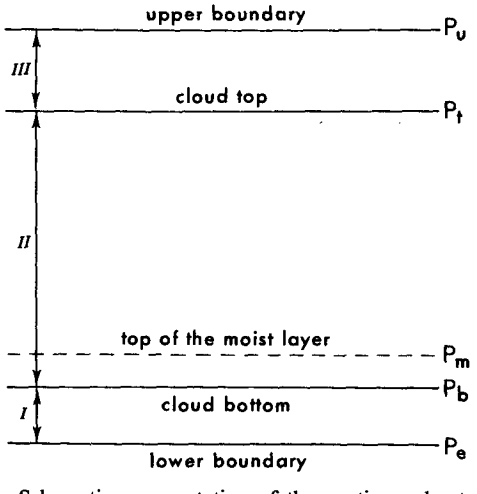

FIG. 1. Schematic representation of the continuously stratified model. I, II and III denote regions below, within and above the cloud, respectively.

The system (2.1) with (2.3) can be reduced to a time-dependent equation for ω:

$$L_1 \frac{\partial^2 \omega}{\partial p^2} - 2 \frac{dU}{dp} \frac{\partial^2 \omega}{\partial x \partial p} + \frac{\sigma}{f_0^2} L_1 \frac{\partial^2 \omega}{\partial x^2} = -\frac{\tilde{\alpha} R L_c \bar{q}}{f_0^2 C_p p_0} \frac{\eta(p)}{p} L_1 \frac{\partial^2}{\partial x^2} \omega(p_m), \tag{2.5a}$$

where we assumed a constant surface evaporation rate, and where the linear operator

$$L_1 \equiv \frac{\partial}{\partial t} + U \frac{\partial}{\partial x}. \tag{2.5b}$$

The lower boundary condition (2.4b) may be rewritten as

$$L_1 \omega + \rho_0 g \left(\frac{K f_0}{2}\right)^{1/2} \frac{\partial \omega}{\partial p} = 0, \quad \text{at} \quad p = p_e. \tag{2.6}$$

In this formulation, the convective latent heating is related to the vertical velocity at the top of the moist convergence layer, $\omega(p_m)$. It essentially reduces to an Ekman–CISK scheme for the case of $p_m = p_e$ and to a conventional wave–CISK scheme in the absence of Ekman layer dynamics. The major feature of interest in the present formulation is that p_m is treated as a parameter that is independent of p_e and p_b, and allowed to be either above or below the cloud base p_b. Therefore, $\omega(p_m)$, which measures the low level convergence, is, in general, controlled by (i) Ekman layer pumping, (ii) geostrophic forcing (when the zonal flow is baroclinic) that is proportional to the product of the vertical shear and horizontal gradient of the vorticity field, and (iii) convective heating field that partly drives the wave motion. In so doing, the direct feedback of the latent heating on the synoptic scale disturbances is included in our model.

3. General eigenvalue problem and its solution

We seek normal mode solutions of the form

$$\omega = \Omega(p) e^{ik(x-ct)} + c.c. \tag{3.1}$$

where $c.c.$ denotes the complex conjugate, and c is the complex phase speed. Substitution of (3.1) into (2.5a) and the boundary conditions (2.4a), (2.6) leads to

$$\frac{d^2\Omega}{dp^2} - \frac{2(dU/dp)}{U(p) - c} \frac{d\Omega}{dp} - S(p) k^2 \Omega = -Q k^2 \frac{\eta(p)}{p} \Omega(p_m), \tag{3.2}$$

$$\Omega = 0, \quad \text{at} \quad p = p_u, \tag{3.3a}$$

$$\Omega - \frac{ir}{k(U - c)} \frac{d\Omega}{dp} = 0, \quad \text{at} \quad p = p_e, \tag{3.3b}$$

where P_0, L, V and $\Omega_0 \equiv (P_0 V^2 / f_0 L^2)$ have been used to scale the pressure, horizontal length, horizontal ve-

locity and vertical p-velocity, respectively. We have also assumed $U - c \neq 0$, since we are interested in the unstable modes. The nondimensional numbers found in (3.2) and (3.3) are

$$\text{the Burger number,} \quad S(p) = \frac{\sigma(p)P_0^2}{f_0^2L^2}, \tag{3.4a}$$

the nondimensional specific humidity,

$$Q = \bar{q}\frac{RL_c}{C_p f_0^2 L^2}, \tag{3.4b}$$

and a measure of the Ekman dissipation,

$$r = \frac{\rho_0 gL}{2P_0V}\left(\frac{Kf_0}{2}\right)^{1/2}. \tag{3.4c}$$

The right-hand side of (3.2) is different from zero only in the cloud region, since $\eta(p) = 0$ outside the cloud. If the basic state is a continuous flow field, one must require that perturbation pressure and vertical velocity be continuous at the upper- and lower-cloud boundaries. Therefore, at the cloud boundaries, the interfacial dynamic and kinematic boundary conditions require that

$$\Omega \text{ is continuous, at } \quad p = p_b, p_t, \tag{3.5a}$$

$$\frac{d\Omega}{dp} \text{ is continuous, at } \quad p = p_b, p_t. \tag{3.5b}$$

Equations (3.2), (3.3a, b) and (3.5a, b) constitute the eigenvalue problem for the complex phase speed c. Before specifying the basic zonal flow and the heating profile, we derive the general dispersion equation for c and an expression for the eigenfunction $\Omega(p)$.

Assume that $\Omega_1(p)$ and $\Omega_2(p)$ are two fundamental solutions of the Eq. (3.2) when $\eta(p) = 0$. We then construct two solutions:

$$f_1(p) = [\Omega_2(p_e)\Omega_1(p) - \Omega_1(p_e)\Omega_2(p)] - \frac{ir}{k(U(p_e) - c)}[\Omega_2'(p_e)\Omega_1(p) - \Omega_1'(p_e)\Omega_2(p)], \tag{3.6a}$$

$$f_2(p) = \Omega_2(p_u)\Omega_1(p) - \Omega_1(p_u)\Omega_2(p), \tag{3.6b}$$

such that $f_1(p)$ and $f_2(p)$ satisfy the lower- and upper-boundary conditions (3.3a, b), respectively; in these expressions, a prime denotes a derivative with respect to p. The Wronskian is

$$W_R(f_1, f_2) = f_1(p_u)W \neq 0, \tag{3.7a}$$

where

$$W \equiv \Omega_1'(p)\Omega_2(p) - \Omega_2'(p)\Omega_1(p). \tag{3.7b}$$

In terms of the homogeneous solutions $f_1(p)$ and $f_2(p)$, we arrive at the following dispersion equation and eigenfunction, which are derived in Appendix A:

$$f_1(p_u) - Qk^2\left[I + f_1(p_m)\int_{p_t}^{p_b}\frac{\eta(t)f_2(t)}{tW(t)}\,dt\right] = 0, \tag{3.8}$$

$$\Omega(p) = \begin{cases} f_1(p), & p_e \geq p \geq p_b, \\ \dfrac{k^2Qf_1(p_m)}{f_1(p_u) - QIk^2}\left[f_1(p)\displaystyle\int_{p_t}^{p}\frac{\eta(t)f_2(t)}{tW(t)}\,dt - f_2(p)\int_{p_b}^{p}\frac{\eta(t)f_1(t)}{tW(t)}\,dt\right], & p_b \geq p \geq p_t \\ \dfrac{k^2Qf_1(p_m)}{f_1(p_u) - QIk^2}f_2(p)\displaystyle\int_{p_t}^{p_b}\frac{\eta(t)f_1(t)}{tW(t)}\,dt, & p_t \geq p \geq p_u, \end{cases} \tag{3.9}$$

where

$$I = \begin{cases} 0, & p_e \geq p_m \geq p_b \\ \displaystyle\int_{p_m}^{p_b}\frac{\eta(t)}{tW(t)}[f_1(t)f_2(p_m) - f_2(p)f_1(p_m)]dt, & p_b > p_m > p_t. \end{cases} \tag{3.10}$$

Once the basic state, i.e., $U(p)$, $\sigma(p)$, and the heating profile $\eta(p)$ are specified, and the two fundamental solutions of the dry problem, $\Omega_1(p)$ and $\Omega_2(p)$, are obtained, we get an analytical expression for the dispersion equation (3.8) and the eigenfunction (3.9).

4. The moist baroclinic wave in the presence of convective heating

a. The dispersion equation and eigenfunction

We now focus our attention on the instability of a moist baroclinic zonal flow with a conditionally unstable layer. For analytical tractability, we assume that the static stability and the vertical shear of the basic zonal flow are constants, i.e.,

$$\sigma(p) = \bar{\sigma}, \tag{4.1a}$$

$$U(p) = 1 - p, \tag{4.1b}$$

where the zonal velocity at the ground ($p = 1$) is assumed to be zero, and the velocity has been scaled by $\lambda_* P_0$, where λ_* is the dimensional vertical shear. Therefore, the basic state, in the absence of convective heating, reduces to Eady's (1949).

The nondimensional heating profile is specified by

$$\eta(p) = \begin{cases} 0, & p_b < p \leq p_e \\ \dfrac{12}{(p_b - p_t)^4}[a(p_b - p)(p - p_t)^2 + (1 - a)(p_b - p)^2(p - p_t)], & p_t \leq p \leq p_b \\ 0, & p_u \leq p < p_t, \end{cases} \tag{4.2}$$

where the shape parameter a is such that $0 \leq a \leq 1$. Figure 2 shows the heating profile defined by (4.2) for different values of a. For $a = 0.5$, $\eta(p)$ is symmetric,

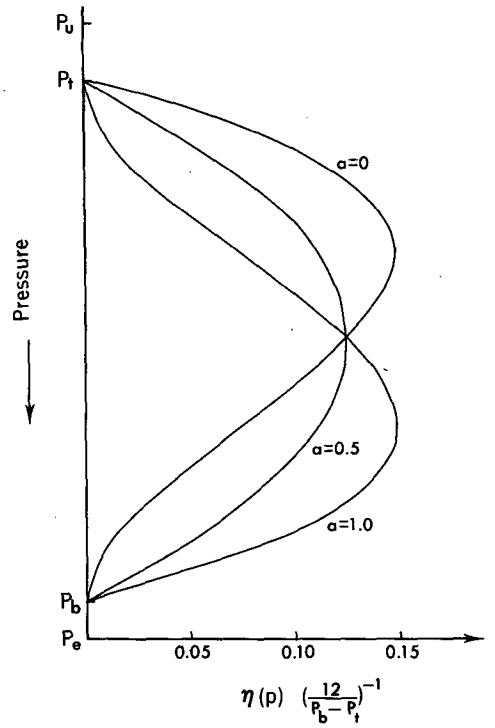

FIG. 2. The vertical heating profile $\eta(p)$ defined by Eq. (4.2).

and as a increases from 0 to 1, the location of the maximum heating decreases from the upper part of the cloud to the lower part of the cloud, while the total area under the curve $\eta(p)$ remains unity.

With the specification of the basic flow (4.1a, b) and the vertical heating distribution, Eq. (3.2) becomes

$$\frac{d^2\Omega}{dp^2} - \frac{2}{p-1+c}\frac{d\Omega}{dp} - \mu^2\Omega = Qk^2\frac{\eta(p)}{p}\Omega(p_m), \quad (4.3)$$

where

$$\mu = S^{1/2}k, \quad (4.3a)$$

$$S \equiv \frac{\bar{\sigma}P_0^2}{f_0^2L^2}. \quad (4.3b)$$

Two fundamental solutions of (4.3) with $\eta(p) = 0$ may be written as

$$\Omega_1(p) = \frac{1}{\sqrt{2}}e^{\mu(1-p-c)}[\mu(1-p-c)-1], \quad (4.4a)$$

$$\Omega_2(p) = \frac{1}{\sqrt{2}}e^{-\mu(1-p-c)}[\mu(1-p-c)+1]. \quad (4.4b)$$

By using (3.6a, b), we have

$$f_1(p) = sh\mu(p_e-p)[\mu^2(1-p_e-c)(1-p-c)-1] + \mu(p_e-p)ch\mu(p_e-p) - ir\frac{\mu^2}{k} \times [\mu(1-p-c)ch\mu(p_e-p) - sh\mu(p_e-p)], \quad (4.5a)$$

and

$$f_2(p) = \mu(p_u-p)ch\mu(p_u-p) - [\mu^2(c-1+p_u) \times (1-p-c)+1]sh\mu(p_u-p). \quad (4.5b)$$

Define

$$I_1(p) \equiv \int^p \frac{\eta(t)f_1(t)}{tW(t)}dt, \quad p_t \leqslant p \leqslant p_b \quad (4.6a)$$

$$I_2(p) \equiv \int^p \frac{\eta(t)f_2(t)}{tW(t)}dt, \quad p_t \leqslant p \leqslant p_b. \quad (4.6b)$$

[$I_1(p)$ and $I_2(p)$ are given in Appendix B.] Then, the dispersion equation becomes

$$f_1(p_u) - Qk^2\{I + f_1(p_m)[I_2(p_b) - I_2(p_t)]\} = 0, \quad (4.7)$$

where

$$I = \begin{cases} 0, & p_e \geqslant p_m \geqslant p_b \\ f_2(p_m)[I_1(p_b) - I_1(p_m)] & \\ -f_1(p_m)[I_2(p_b) - I_2(p_m)], & p_b > p_m > p_t. \end{cases} \quad (4.8)$$

The eigenfunction is given by

$$\Omega(p) = \begin{cases} f_1(p), & p_e \geqslant p > p_b \\ Qk^2\dfrac{f_1(p_m)}{f_1(p_u) - Qk^2I}\{f_1(p)[I_2(p) - I_2(p_t)] & \\ \quad - f_2(p)[I_1(p) - I_1(p_b)]\}, & p_b \geqslant p \geqslant p_t \\ Qk^2\dfrac{f_1(p_m)}{f_1(p_u) - Qk^2I}f_2(p)[I_1(p_b) - I_1(p_t)], & \\ & p_t > p \geqslant p_u. \end{cases}$$

When the moisture content $\bar{q} = 0$, (4.7) reduces to $f_1(p_u) = 0$, which recovers Eady's dispersion equation if the Ekman dissipation is set to zero. The dispersion equation (4.7) for a general heating profile (4.2) is a complex transcendental equation involving logarithmic functions and infinite power series which can be truncated in numerical calculation because of its fast convergence. This equation is similar to the one obtained in a previous work and can be solved by iteration (Wang et al., 1986). The analytical technique employed here enables us to obtain our results with a significant reduction in the amount of computation and to study the instability properties extensively.

b. *The characteristics of the instability*

Figure 3a, b shows the growth rate and phase speed as functions of wavenumber k and specific humidity $\bar{q}$, respectively. Points k_m and k_c on the $\bar{q} = 0$ axis indicate the most unstable and the cutoff wavenumbers of the Eady problem, respectively. From Fig. 3 several conclusions can be drawn:

1) The long waves with characteristic length scale longer than Rossby radius of deformation ($k < k_m$) are

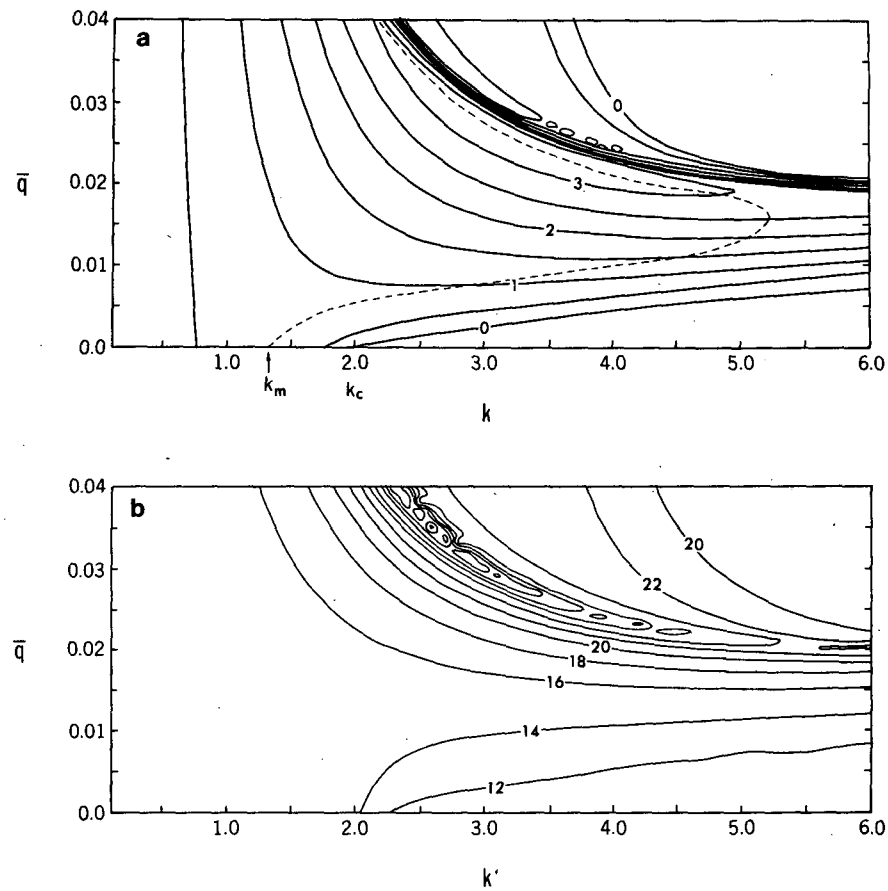

FIG. 3. (a) The growth rate (day^{-1}) and (b) the phase speed (m s^{-1}) of the wave disturbances for a general heating profile (4.2), as functions of the wavenumber (wavelength) and the averaged specific humidity of the moist layer $\bar{q}$ computed from (4.7). The dashed line shows the preferred wavenumber. All the parameters have the values listed in section 5 except $P_u = 0$ mb, $\bar{\sigma} = 0.015$ m^2 s^{-2} mb^{-2}.

not affected appreciably by convective latent heating. Dramatic increases in the growth rate and phase speed are mainly found in the short waves with characteristic horizontal length scales less than the Rossby radius of deformation.

2) For a given moisture content $\bar{q}$, the instability spectrum (i.e., the dependence of the growth rate on the wavenumber) is characterized by a preferred wavenumber (or wavelength) that corresponds to the maximum growth rate. The preferred wavelength is a nonlinear function of the moisture content $\bar{q}$, as depicted by the dashed line in Fig. 3a. An optimum value of $\bar{q}$ exists that minimizes the preferred wavelength; we shall refer to it as the optimum specific humidity, $\hat{q}$. As will be seen in Fig. 5, there is another value of $\bar{q}$ that maximizes the growth rates of the most unstable waves. The later is, in general, slightly larger than the optimum specific humidity $\hat{q}$.

3) There is a clear boundary between growing and decaying wave regions which represents the neutral waves. It is noted that when the moisture content exceeds its optimum value $\hat{q}$, there exists a minor growing wave region next to the major unstable region, in which the maximum growth rate is smaller than that found in the major unstable region.

The qualitative picture of the moist baroclinic instability associated with cumulus convective heating shown in Fig. 3 does not change when we vary the parameters used in the calculation. However, the characteristics of the instability spectrum, i.e., the growth rate and wavelength of the most unstable mode and cutoff wavelength, do vary with the basic zonal flow properties (vertical shear, static stability and rotation rate) and the vertical heating distribution, $\eta(p)$. These dependencies will be examined in the next section. Although the baroclinic forcing contributes to the initiation of the convection, a certain amount of moisture content, $\bar{q}$, is required for the free development of a feedback process of convection. Therefore, we should deemphasize the significance of the results obtained for small values of $\bar{q}$ in Fig. 3.

It is important to point out that the optimum specific humidity $\hat{q}$ strongly depends upon the static stability of the basic flow for given $\eta(p)$. Table 1 indicates the relationship between the optimum specific humidity and the static stability of the zonal flow for a representative tropospheric heating profile. The optimum specific humidity in Table 1 is proportional to the static stability. When the specific humidity reaches its optimum value, the characteristic length scale of the unstable mode, L, is significantly smaller than the Rossby radius of deformation, $L_D = \bar{\sigma}^{1/2}P_0/f_0L$, i.e., the Burger number $S = L_D^2/L^2 \gg 1$. From the nondimensional quasi-geostrophic ω-equation,

$$\frac{\partial^2\omega}{\partial p^2} + S\frac{\partial^2\omega}{\partial x^2} = 2\frac{dU}{dp}\frac{\partial^2\phi}{\partial x^2} + Q\frac{\eta}{p}\frac{\partial^2\omega(p_m)}{\partial x^2},$$

which was derived from Eq. (2.1a, b) with (2.3), the basic balance must be between the second term on lhs and the last term on rhs, i.e., the vertical velocity is chiefly produced by cumulus latent heating. If we equate the Burger number S and nondimensional specific humidity Q [see (3.4a, b)], then

$$\hat{q} = \frac{C_p}{R}\frac{\bar{\sigma}P_0^2}{L_c},$$

which gives an approximate expression of this proportionality. If we express $Q = L_h^2/L^2$ [see (3.4b)] where $L_h \equiv (\bar{q}L_cR/f_0^2C_p)^{1/2}$ can be regarded as a characteristic horizontal length scale associated with cumulus heating, then the optimum specific humidity makes the characteristic heating length scale, L_h, roughly equal the Rossby radius of deformation.

The existence of an upper (lower) bound in the growth rate (wavelength) of the most unstable wave was noticed earlier and considered to be a consequence of Mak's (1982) parameterization, which is different from the wave–CISK scheme. In the absence of the Ekman dynamics and when $p_m = p_b$, as the case in Fig. 3, the present parameterization is essentially the same as the traditional wave–CISK treatment. Yet, the behaviors of the variation with heating intensity for the growth rate and wavelength of the most unstable mode are still fundamentally different from those of conventional, inviscid, tropical wave CISK modes, for which the growth rate increases with increasing wavenumber and no finite preferred spatial scale exists (Hayashi, 1970).

TABLE 1. The dependence of the optimum specific humidity $\hat{q}$ on static stability $\bar{\sigma}$ for a representative heating profile (p_e = 1000 mb, p_u = 300 mb, $p_b = p_m$ = 900 mb, p_t = 400 mb, $0 \leq a \leq 1$).

$\bar{\sigma}$ ($m^2\ s^{-2}\ mb^{-2}$)	$\hat{q}$ ($g\ kg^{-1}$)	L_{min} (km)
0.015	0.016	1150
0.02	0.021	1340
0.03	0.031	1610
0.04	0.041	1900

c. *The dynamic nature of the baroclinic wave CISK mode*

In a baroclinic zonal flow, the low-level moisture convergence is sustained by baroclinic wave forcing and latent heat release in the absence of Ekman pumping. The unstable mode shown in Fig. 3 is, therefore, referred to as baroclinic wave CISK mode.

If we now consider a simplified heating profile used by Mak (1982)

$$\eta(p) = \begin{cases} 0, & \text{outside the cloud} \\ \dfrac{2}{p_b^2 - p_t^2}p, & p_t \leq p \leq p_b, \end{cases} \tag{4.9}$$

then the dispersion equation (3.8) reduces to

$$f_1(p_u) - \frac{2Q}{(p_b^2 - p_b^2)S\mu}\frac{f_1(p_m)}{(p_t + c - 1)(p_b + c - 1)} \times \{(p_t + c - 1)[\mu(p_u + c - 1)ch\mu(p_b - p_u) + sh\mu(p_b - p_u)] - (p_b + c - 1)[\mu(p_u + c - 1) \times ch\mu(p_t - p_u) + sh\mu(p_t - p_u)]\} = 0, \tag{4.10}$$

where $f_1(p)$ is defined by (4.5a). The growth rate from (4.10) is given in Fig. 4, where all the parameters used in the figure are identical to those in Fig. 3. In general, the results from both heating profiles are rather similar. However, the preferred wavenumber and cutoff wavenumber are influenced by the heating profile, especially near the optimum specific humidity $\hat{q}$. Nevertheless, the results derived by using a simplified heating profile do capture the qualitative features reflected in Fig. 3a. Therefore, we may use the dispersion equation (4.10) to discuss the qualitative nature of the unstable modes.

When $\bar{q} = 0$, the roots of (4.10) give two unstable (complex conjugate) Eady modes. When $\bar{q} \neq 0$, the two unstable Eady modes are remarkably modified by latent heat release, while there are another two modes that remain neutral. Therefore, the baroclinic wave CISK mode can be viewed as baroclinic wave intensified by latent heat release. Furthermore, as shall be seen in the next section, the fundamental dependency of dry baroclinic instability on the static stability, rotation rate and vertical shear remain qualitatively valid in the presence of convective latent heating.

Mak (1982) proposed a conceptually different formulation based on the premise that the cooperative heating feedback is only associated with the baroclinically induced low-level convergence. Therefore, the scale selection mechanism in his model was believed to result from the heating not being expressed in terms of the vertical velocity, per se, as in the usual wave CISK treatment. This formulation neglected the low-level convergence directly induced by latent heat release

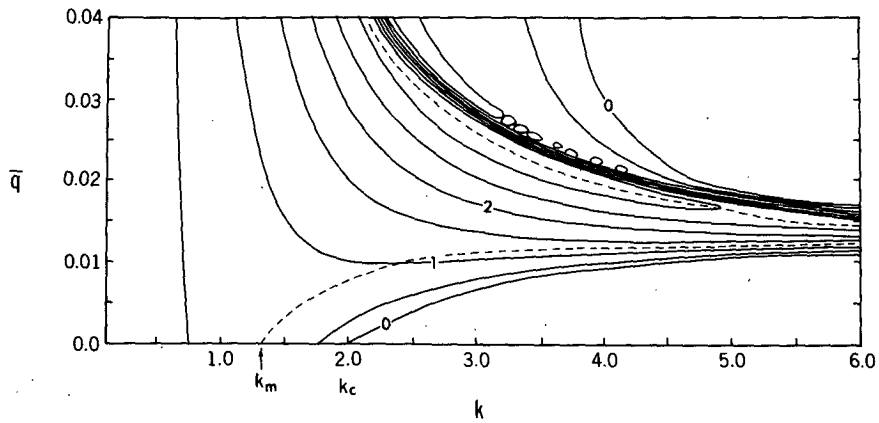

FIG. 4. As in Fig. 3a, but for the simplified heating profile (4.9).

and may be inconsistent with the fact that low-level convergence is partly driven by latent heat. In the present formulation, the moisture convergence is not due solely to the rotational part of the wind field, but is also due to the interactive diabatic heating. Moreover, we consider the general case in which the top of the moist layer may be above the cloud base, so that the direct feedback of the heating on the low-level moisture convergence is included. The results reveal the existence of a spatial scale selection, in contrast to the results for the conventional wave CISK in an ageostrophic model with no basic flow or with a uniform basic flow. The present study suggests that, in the presence of baroclinic instability, the cooperative heating feedback need not be parameterized only in terms of the dynamically induced low-level convergence so as to ensure an appropriate scale selection mechanism in the moist instability of a baroclinic zonal flow associated with CISK.

As Mak (1983a) noticed, the scale selection is probably affected, to some extent, by the CISK formulation itself, especially in layer models. Nevertheless, if the effect of the conditionally unstable stratification is parameterized with the assumption that the amount of heat released is proportional to the vertical velocity at the top of the moist convergence layer, as used here and in many other studies, the quasi-geostrophic balance and baroclinity of the zonal flow are decisive factors for suppressing the short-scale waves and lead to a finite preferred wavelength in a continuously stratified model. As has been pointed out previously, the baroclinic wave CISK mode can be regarded as a modified baroclinic wave, and the wave selection mechanism seems to be rooted in the baroclinic instability; the convective latent heating with the present parameterization does not change this property qualitatively.

5. Influential factors controlling instability and possible mechanism for explosive growth

A series of experiments was carried out to examine the influences of each physical factor. In all calculations, unless specified otherwise, the parameters are given the following typical values:

$\lambda_* = 0.03$ m s^{-1} mb^{-1},	vertical shear
$\bar{\sigma} = 0.02$ m^2 s^{-2} mb^{-2},	static stability parameter
$f_0 = 10^{-4}$ s^{-1},	coriolis parameter
$K = 0$ m^2 s^{-1},	eddy viscosity coefficient in the Ekman layer
$p_e = 1000$ mb,	pressure at the lower boundary
$p_u = 300$ mb,	pressure at the upper boundary
$p_b = 900$ mb,	pressure at the cloud base
$p_t = 400$ mb,	pressure at the cloud top
$p_m = 900$ mb,	pressure at the top of moist layer
$a = 0.5$,	profile parameter.

a. *The influences of the static stability, rotation rate and vertical shear*

The curves in Fig. 5 depict the instability characteristics as a function of $\bar{q}$ for $\bar{\sigma} = 0.02$ and 0.015 m^2 s^{-2} mb^{-2}. Reduced static stability enhanced growth rates of the most unstable modes for all $\bar{q}$. Furthermore, the optimum specific humidity which minimizes preferred wavelength was also reduced. In the realistic range of $\bar{q}$ ($\bar{q} < 0.02$), the destabilizing effects of the latent heat release was significantly enhanced by the reduced static stability. For example, the ratio of the moist maximum growth rate ($\bar{q} = 0.01$) to the dry maximum growth rate ($\bar{q} = 0$) is 1.72 for $\bar{\sigma} = 0.02$ m^2 s^{-2} mb^{-2}, in comparison to the value of 2.23 for $\bar{\sigma} = 0.015$ m^2 s^{-2} mb^{-2}. The reduced static stability catalyzes the destabilizing effect of the latent heat release and induces a dramatic increase in growth. In a dry baroclinic model ($\bar{q} = 0$) the reduction of static stability from 0.02 to 0.015 m^2 s^{-2} mb^{-2} causes an increase in growth rate by 17%, while the same reduction of static stability induces an increase in growth rate by about 54% when $\bar{q} = 0.01$. Therefore, the effect of reduced static stability on the

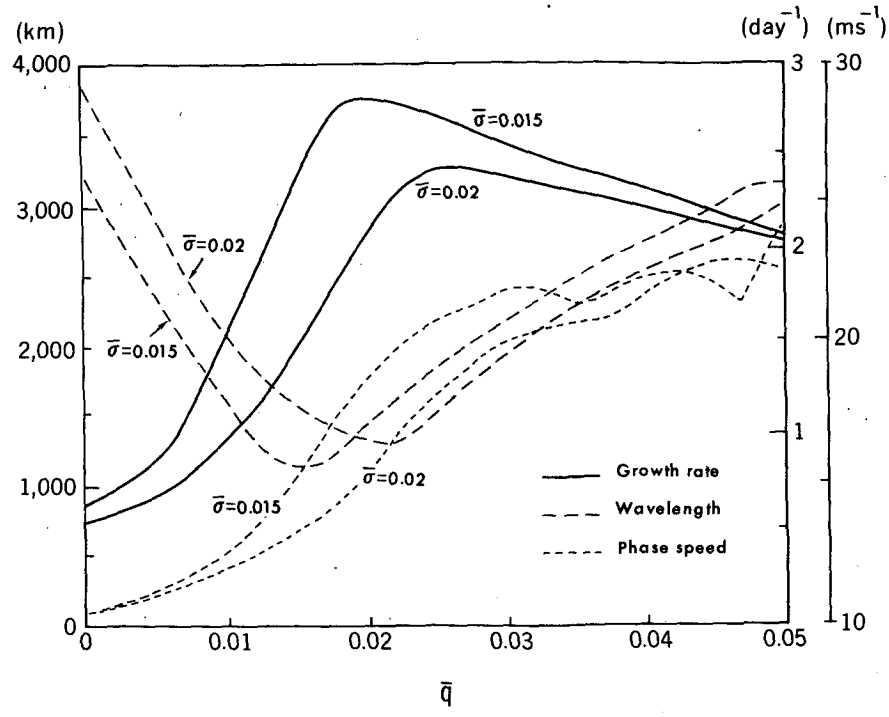

FIG. 5. The growth rate, wavelength, and phase speed of the most unstable modes, as functions of averaged specific humidity of the moist layer $\bar{q}$ for $\bar{\sigma}$ = 0.015 and 0.02 m^2 s^{-2} mb^{-2}. The general heating profile (4.2) is used. All other parameters are given the same values as listed in section 5.

instability was intensified by the convective latent heat release. There exists a mutual cooperative interaction between the destabilizing effects of reduced static stability and increased latent heat release.

Table 2 shows how the rotation rate influences the instability. The ratio of moist maximum growth rate ($\bar{q}$ = 0.01) to dry maximum growth rate is about the same (1.73) for the four listed different rotation rates. In a dry baroclinic Eady model, a faster rotation rate ensures that the shorter waves are the fastest growing. This effect remains valid as latent heat is included and in the presence of an Ekman layer. In the present cases, the destabilizing influence of the increased rotation rate is rooted in the dry baroclinic instability and is transferred to the moist baroclinic instability; it is not enhanced by the latent heat release. For dry inviscid baroclinic instability, the growth rate is proportional to the vertical shear for a given Burger number. With the parameterized convective latent heating, the growth rate remains proportional to the vertical shear for a fixed Burger number, moisture content $\bar{q}$, and heating profile. Moreover, the growth rate does not change when the sign of the vertical shear reverses in both the dry model and the moist model. This property holds for an f-plane model. In summary, the above findings are further manifestations that the baroclinic wave CISK mode is a baroclinic wave strongly modified by the convective heating.

TABLE 2. Variations of the instability characteristics with increasing rotation rate for dry ($\bar{q}$ = 0) and moist ($\bar{q}$ = 0.01) cases. All other parameters are assigned their typical value.

		Most unstable mode			
$\bar{q}$	f_0 (10^{-4} s^{-1})	Wavelength (km)	Growth rate (day^{-1})	Phase speed (m s^{-1})	Cutoff wavelength (km)
0.0	0.5	7850	0.28	10.5	4830
	0.707	5500	0.40	10.5	3930
	1.0	3950	0.57	10.5	2510
	1.22	3200	0.69	10.5	2090
0.01	0.5	4190	0.49	12.0	2330
	0.707	3000	0.69	12.0	1700
	1.0	2170	0.98	11.9	1190
	1.22	1800	1.19	11.9	<1000

b. *The influence of the vertical heating distribution*

The present cumulus parameterization scheme, (2.3), applies to the deep precipitating cumulus convection. The total amount of latent heat is controlled by low-level, large-scale moisture convergence, yet the height of the cloud top varies from place to place, depending upon the thickness of the conditionally unstable layer and upon the environmental moisture content at mid- and upper-levels, as well.

Table 3 compares the characteristics of the most unstable modes for $\bar{q}$ = 0.01 for p_t = 300, 400, 500 mb.

TABLE 3. Variations of the characteristics of the most unstable mode with decreasing cloud top for $\bar{q} = 0.01$. All other parameters are assigned their typical values.

Pressure at the cloud top (mb)	Most unstable mode		
	Wavelength (km)	Growth rate (day^{-1})	Phase speed ($m\ s^{-1}$)
300	2510	0.84	12.0
400	2170	0.98	11.9
500	1650	1.21	11.2

The result shows that the lower cloud top may result in much stronger growth in shorter waves and slower wave propagation. In relatively shallow convection, the cloud layer is relatively thin and the intensity of the maximum heating is larger than that of the deeper convection [see Eq. (4.2)], the heating being released in the lower atmospheric layer. The strong low-level heating, on one hand, tends to strengthen moisture convergence into the cloud and stimulate latent heat release; on the other hand, it tends to lower the steering level of the unstable mode so as to slow down the wave propagation. Since the shorter waves have a shallow vertical scale, they are more readily affected by the enhanced low-level heating.

When the cloud top and base are fixed, the shape of the heating profile is found to change the instability slightly. Table 4 indicates that the heating with a maximum below the cloud center ($a = 1$) has a similar influence as that of lower cloud top, i.e., it destabilizes the shorter waves and reduces the propagation speed.

An increase in the location of the upper boundary (p_u smaller) slightly increases the growth rate, in general, if other parameters are unchanged. It also increases the wave speed by raising the steering level for the unstable mode.

c. *Deep versus shallow moist convergence layer*

Observations show that the conditionally unstable layer may be close to the ground, i.e., the cloud base may be lower than the top of the moist convergence layer. In the present model, we refer to that case as the "deep moist layer," while the "shallow moist layer" has the top of the moist layer below or at cloud base.

TABLE 4. Variations of the characteristics of the most unstable mode with changing location of the maximum heating. All other parameters are assigned their typical values ($\bar{q} = 0.01$).

Heating profile parameter a	Most unstable mode		
	Wavelength (km)	Growth rate (day^{-1})	Phase speed ($m\ s^{-1}$)
0.0	2030	1.00	12.9
0.5	2170	0.98	11.9
1.0	1790	1.10	11.0

In the model with a shallow moist layer, since $\eta(p_m) = 0$, the low-level, large-scale convergence is not directly affected by latent heating. In the deep moist layer case, $\eta(p_m) \neq 0$, and the convective heating has a *direct* feedback on the low-level moisture convergence.

If we assume the cloud base $p_b = 950$ mb, the eddy viscosity coefficient $K = 5\ m^2\ s^{-1}$, the lower boundary $p_e = 950$ mb, and all other parameters have the values listed earlier, the calculated growth rates for $\bar{q} = 0$, 0.005 and 0.01 are shown in Fig. 6. For the same moisture content, the deeper moist layer produces a larger growth rate and a shorter preferred wavelength. When the top of the moist layer extends above cloud base, the instability spectrum retains its single peak feature for smaller $\bar{q} = 0.005$ but exhibits a double peak for $\bar{q} = 0.01$, with one peak appearing in the wavelength around 1300 km, beyond which there is a sharp decrease in the growth rate with wavenumber. Figure 7 compares the results for two inviscid cases for 1) $p_b = 950$ mb and 2) $p_b = 900$ mb, all other parameters having the values listed earlier. In case 1 the cumulus heating directly controls the low-level moisture supply (since $p_m < p_b$), though the actual depth of the moist layer is the same as that in case 2. We see that for smaller $\bar{q}$ (=0.005), the growth rates in both cases do not differ appreciably. When $\bar{q} = 0.01$, the growth rate in case 1 has two peaks, and the maximum growth rate (1.11 day^{-1}) is larger than that in case 2 (0.98 day^{-1}), while the preferred wavelength in case 1 is much shorter (1230 km) than that in case 2, which is 2170 km. There is a sharp decrease in growth rate in the short wave side of the preferred wavelength. If the moisture content and the moisture layer depth become large enough, a singularity will occur for certain wavenumber, because the denominator in (A7) would tend to zero, and the vertical velocity at the top of the moist convergence

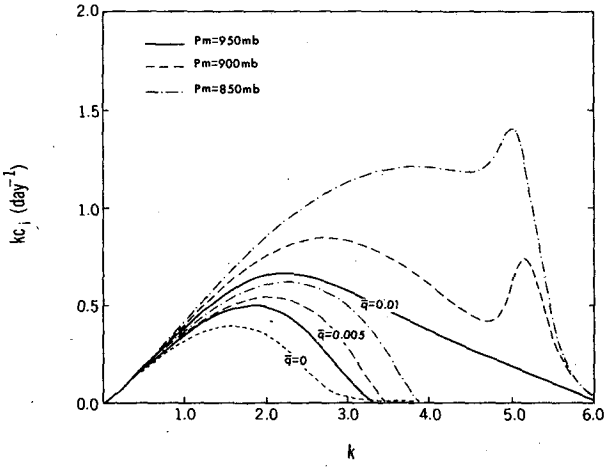

FIG. 6. The growth rates for the heating profile (4.2) as functions of wavenumber for different moist layer depth. The top three curves correspond to averaged specific humidity $\bar{q} = 0.01$. All parameters have the same values listed in section 5, except $K = 5\ m^2\ s^{-1}$.

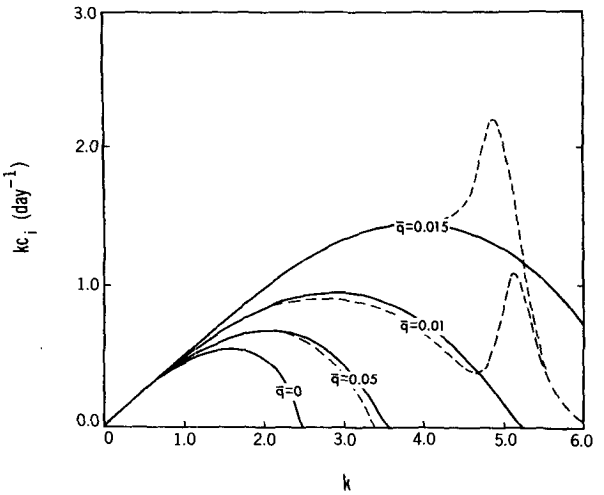

FIG. 7. The variations of the growth rate with wavenumber for cases of 1) P_b = 900 mb (solid curves) and 2) P_b = 950 mb (dashed curves). All other parameters have the values listed in section 5.

layer would tend to infinite. This singularity is essentially similar to that found in Charney and Eliassen's (1964) model (Mak, 1981) and reflects the limitations of the present cumulus parameterization scheme. Nevertheless, the singularity occurs only in an unrealistic parameter range.

d. *The effect of the Ekman layer*

The lower boundary condition of the inviscid interior region was applied at the top of Ekman layer, p_e, where the vertical velocity is assumed to match Ekman pumping velocity ω_e. Because the Ekman layer has a finite thickness, the vertical velocity at p_e is produced by both baroclinic wave and Ekman pumping. If we assume the top of the moist layer at p_m = 900 mb and apply the boundary condition $\omega = \omega_e$ at 900 mb, we underestimate the actual vertical velocity at this level, because we neglect the vertical velocity induced by baroclinic wave; if we use the lower boundary condition at 1000 mb (surface), we overestimate the vertical velocity at 900 mb, because we neglect the thickness of the boundary layer. To include both contributions to vertical velocity at the top of the moist layer, we apply the lower boundary condition at 950 mb.

Figure 8 shows how the Ekman layer affects the growth rates for different moisture contents $\bar{q}$. In the presence of moisture, Ekman layer pumping, on one hand, produces vortex compression or stretching in such a way as to weaken the eddy vorticity; on the other hand, it contributes to the eddy development via low-level moisture convergence. As the low-level moist layer contains more moisture, the positive contribution of the Ekman pumping becomes more prominent. As shown in Fig. 8, when $\bar{q}$ increases, the growth rate has a larger increase in the presence of Ekman pumping than in its absence, especially when the Ekman layer friction is enhanced. For example, the ratios of the moist maximum growth rate at $\bar{q}$ = 0.01 over that at $\bar{q}$ = 0 are 1.72, 2.28 and 2.89 for K = 0, 5 and 12 m^2 s^{-1}, respectively. Note that in the absence of cumulus heating, the Ekman layer reduces the maximum growth rate by nearly a factor of two as K = 12 m^2 s^{-1}, while with moderate cumulus heating ($\bar{q}$ = 0.01) the Ekman layer increases the maximum growth rate by about 10%.

The presence of the Ekman layer dissipation also slows down the phase speed of wave propagation for all unstable modes. For $\bar{q}$ = 0.01, the phase speeds of the most unstable modes are 11.9, 10.9 and 10.8 m s^{-1} for K = 0, 5 and 12 m^2 s^{-1}, respectively.

e. *The combined effects and explosivelike growth*

The explosive cyclogenesis was defined as a depression with a deepening rate of at least 24 mb day^{-1}; some extra large deepening rates even reach 60 mb day^{-1} (Sanders and Gyakum, 1980). The explosive growth rate is about 2 to 5 times that of the usual dry baroclinic growth rate.

If we consider the static stability $\bar{\sigma}$ = 0.02 m^2 s^{-2} mb^{-2}, the increases of the maximum growth rate are about 23%, 72% and 156% of the corresponding dry one as $\bar{q}$ = 0.005, 0.01 and 0.015, respectively. (See Fig. 5.) In general, the averaged specific humidity of the moist layer in a midlatitude cyclone region is about 5 ~ 10 g kg^{-1}. The increase in maximum growth rate is, therefore, not large enough to account for the explosive growth. Our estimate is close to that of Sardie and Warner (1983), but is substantially smaller than Mak's (1982). The apparent reason for the later disagreement is that Mak used a larger heating intensity coefficient.

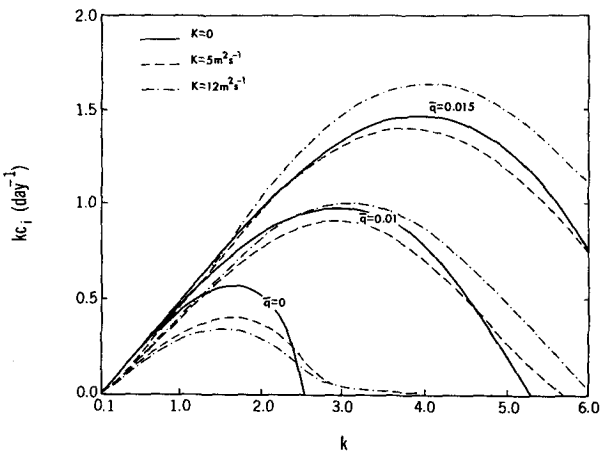

FIG. 8. The growth rates for the heating profile (4.2) as functions of wavenumber for different Ekman layer friction. Three groups of curves correspond to $\bar{q}$ = 0, 0.01 and 0.015, respectively. All other parameters are the same as those listed in section 5.

If we use Mak's heating profile, Eq. (4.9), we find that his heating intensity is given by

$$\epsilon = \frac{2L_c}{(p_b^2 - p_t^2)C_p p_0}\,\bar{q},$$

where p_b and p_t are the nondimensional pressures at the cloud base and top, respectively. Using Mak's parameters—$p_b = 0.9$, $p_t = 0.4$ and $P_0 = 1000$ mb—we get $\epsilon \approx 7.7\bar{q}$ (K mb^{-1}). Table 5 compares our model results for $\sigma = 0.04$ m^2 s^{-1} mb^{-2} and $K = 0$ m^2 s^{-1} with Mak's results for the same heating profile and parameters. When $\epsilon \leq 0.2$, the results are close. The discrepancies between the two model results increase as $\bar{q}$ or ϵ increases, suggesting that Mak's CISK formulation, in which the vertical velocity at the top of the moist convergence layer is sustained only by the dynamical field, underestimates the destabilizing effect of the convective heating, especially as $\bar{q}$ approaches the optimum value $\hat{q}$.

As has been discussed, besides the destabilization of increased moisture content, there are a number of favorable factors for rapid development of the disturbances, such as reduced static stability, increased vertical shear, higher latitude, shallower convection, and deeper moist convergence layer with its top above cloud base. These influential factors are reported to be indeed pertinent to the rapid growth. For example, in his analysis of the 18–19 February 1979 storm, Bosart (1981) pointed out that cyclogenesis was initiated along a coastal front, a region of enhanced lower-tropospheric baroclinity due to significant oceanic sensible and latent heat fluxes which warm, moisten and destabilize the boundary layer. Sanders and Gyakum (1980) suggested a cumulus heating profile with a lower tropospheric peak in the intensifying stage of very strong extratropical cyclones. Recently, in his partitioning of the total heating into cumulus and mesoscale components, Johnson (1984) pointed out that the cumulus component produces a heating peak centered near 600 mb (refer to his Fig. 6), which is similar to our shallower convection case. The heating profile is probably dependent on the static stability and the moisture profile in the free atmosphere, which controls the depth of convection. In the incipient stage, a relatively dry free atmosphere in midlatitude would reduce the depth of convection via the entrainment process; the heating profile more likely possesses a lower maximum. With the rapid development, the heat released in the lower troposphere may further destabilize the upper troposphere and promote deep convection.

It is important to point out that the cooperative interaction between favorable factors listed earlier may create large growth which substantially exceeds the linear combination of their individual effects. Two illustrative examples are given in Tables 6 and 7. Table 6 shows that the reduction of the static stability and the depth of convection in isolation may cause an additional 40% and 23% increase, respectively, in the maximum growth rate, compared to the normal convective heating case. However, their joint effect produces an 105% increase in the maximum growth rate, which is

TABLE 5. The growth rate (10^{-5} s^{-1})/wavelength (km) of the most unstable modes computed from Mak's model (estimated from his Fig. 3) and the present models by use of Mak's parameters and his heating profile, Eq. (4.9), ($K = 0$ m^2 s^{-1}, $\sigma = 0.04$ m^2 s^{-2} mb^{-2}).

	ϵ (K mb^{-1})				
	0.1	0.2	0.3	0.4	0.5
Mak's model	0.62 5750	0.78 4600	0.92 4000	1.10 3400	1.30 3050
Present model	0.65 5700	0.87 3950	2.24 1750	2.58 2600	2.54 3150

TABLE 6. Characteristics of the most unstable modes for 1) normal case, 2) shallow convection, 3) reduced static stability, and 4) combination of shallow convection and reduced static stability. $\bar{q} = 0.01$; all other parameters are assigned typical values.

Cases	Most unstable mode		
	Wavelength (km)	Growth rate (day^{-1})	Phase speed (m s^{-1})
1. $p_t = 400$ mb, $\bar{\sigma} = 0.02$ m^2 s^{-2} mb^{-2}	2170	0.98	11.9
2. $p_t = 500$ mb, $\bar{\sigma} = 0.02$ m^2 s^{-2} mb^{-2}	1650	1.21	11.2
3. $p_t = 400$ mb, $\bar{\sigma} = 0.015$ m^2 s^{-2} mb^{-2}	1530	1.47	12.8
4. $p_t = 500$ mb, $\bar{\sigma} = 0.015$ m^2 s^{-2} mb^{-2}	1120	2.01	12.2

TABLE 7. Characteristics of the most unstable modes for 1) normal case, 2) deep moist layer, 3) shallow convection, and 4) combination of relatively deep moist layer and shallow convection. $\bar{q} = 0.01$, $p_b = 950$ mb, $K = 5$ m^2 s^{-1}, $p_e = 950$ mb, other parameters are assigned their typical values.

Cases	Most unstable mode		
	Wavelength (km)	Growth rate (day^{-1})	Phase speed (m s^{-1})
1. $p_m = 950$ mb, $p_t = 400$ mb	2860	0.66	9.8
2. $p_m = 900$ mb, $p_t = 400$ mb	2240	0.84	10.6
3. $p_m = 950$ mb, $p_t = 500$ mb	2240	0.70	8.7
4. $p_m = 900$ mb, $p_t = 500$ mb	1280	1.15	8.4

about 3.5 times that of the dry maximum baroclinic growth rate (0.57 day^{-1}). Table 7 compares the results of the joint effects of shallow convection and deeper moist layer in the presence of Ekman layer dissipation with their individual effects. The increase in maximum growth rate for the combined effect is 74%, which is a good deal larger than that for shallow convection alone (6%) or for a deeper moist layer alone (27%) and is almost 2.9 times the maximum dry baroclinic growth rate (0.40 day^{-1}). Moreover, the phase speed for the combined case is slower than the dry case, which is also a result in line with the observations. For example, the *QEII* storm appears to slow down during its rapid deepening stage (Gyakum 1983a).

Although the model considers only the bulk effect of the cumulus convection, the parameters involved in the model may reflect the indirect impacts of other related relevant physical processes, for example, the sensible heating and boundary layer process (frontogenesis). The strong upward sensible and latent heat fluxes are typically largest during the earliest stage of development of polar lows, i.e., in the region where the enhanced convection originated but not in the region of explosive development (Mullen, 1983). Therefore, as Danard and Elleton (1980) and Bosart (1981) suggested, surface heating may not be directly responsible for explosive cyclogenesis; instead, it serves to establish a favorable low-level environment via the warm and moist boundary layer by increasing the moist content and the thickness of the moist layer, destabilizing the large-scale stratification, and building up a stronger conditionally unstable layer. As shown above, all these effects will contribute positively to the rapid growth of the baroclinic wave–CISK modes. Similarly, the differential heating between warm ocean current and cold continent will enhance the baroclinity in the lower troposphere. The latter, in turn, will increase the growth of the baroclinic wave–CISK mode.

6. Summary and conclusions

A theoretical, linear analysis of the moist instability of a baroclinic zonal flow with conditionally unstable stratification in the presence of an Ekman layer friction is presented. The bulk effect of the cumulus convection is incorporated into the two-dimensional continuous model in an f-plane with the use of the simplified Kuo's scheme and an adjustable heating profile. The vertical velocity employed in the CISK parameterization is consistent with Ekman layer pumping, baroclinic wave forcing, and diabatic heating field. The direct feedback of the latent heat release on synoptic scale disturbances is included.

The general dispersion equation and eigenfunction were derived analytically in terms of the homogeneous fundamental solutions without specification of the basic flow properties and heating profile. The analytical solutions were obtained for a zonal flow with constant vertical shear and static stability, as well as a representative heating profile.

The moist unstable mode of a conditionally unstable, baroclinic zonal flow may be regarded as a modified baroclinic wave by the bulk effect of convective latent heating. The fundamental dependences of the baroclinic growth rate on the static stability, rotation rate and vertical shear remain qualitatively valid for the moist instability of baroclinic flow associated with CISK.

Besides being dependent on the Burger number and the vertical shear, the moist instability under investigation crucially depends on the averaged specific humidity $\bar{q}$ of the moist convergence layer, which measures the latent heating intensity and the moist energy stored in the mean flow. Both available potential energy, measured by vertical shear, and available moist energy, measured by $\bar{q}$ and the depth of the moist convergence layer, are important energy sources for the moist unstable modes. The behavior of the waves longer than the Rossby radius of deformation are not appreciably effected by convective heating, while the waves shorter than the Rossby radius of deformation are significantly destabilized by the convective heating. The characteristics of the unstable spectrum, i.e., the growth rate, and the wavelength of the most unstable mode are nonlinear functions of the moisture content $\bar{q}$. There exist optimum values of $\bar{q}$ that minimize the preferred wavelength and maximize the growth rate. These optimum values are strongly dependent on the static stability of the zonal flow, as well as on the vertical heating distribution. It is found that the optimum specific humidity $\hat{q}$ that minimizes the preferred wavelength for a representative tropospheric heating distribution can be approximately estimated by matching the Rossby radius of deformation with a length scale $L_h \equiv (\bar{q}L_c R/f_0^2 C_p)^{1/2}$ determined by moist energy per unit mass and rotation rate, i.e., $\bar{q}$ is proportional to the static stability.

In contrast to the tropical wave CISK, there is a clear scale selection in the growth rate spectrum of the wave CISK in baroclinic flow, in which the vertical shear plays an essential part. If the moisture convergence is primarily confined in the lower layer, the quasi-geostrophic balance and baroclinity of the basic flow seem to be enough to suppress short waves and lead to a finite preferred wavelength. Therefore, with the present convective heating parameterization, the scale selection appears to be of the same nature as that found in a dry baroclinic model.

The results presented in sections 4 and 5 were based upon the assumptions of constant static stability parameter σ, constant vertical shear, and no β-effect. Mak (1983b) showed that the instability properties of the moist Eady model and the moist Charney model are fundamentally alike and that a more realistic static stability (say an exponential profile) does not change the basic features of the instability process either, although

it can have noticeable quantitative influence upon the characteristics of the instability. It remains to be investigated whether the preferred scale is explained by the baroclinic wave CISK when realistic vertical and horizontal shears are used. In particular, a constant shear without β-effect gives spuriously distinct short wave cutoff.

The destabilizing effect of the latent heat release was found to be remarkably enhanced when the static stability of the basic flow is reduced by other processes, say strong upward oceanic sensible and latent heat fluxes. Besides the reduced static stability, the following factors may also have a significant influence on the maximum growth rate and the preferred wavelength: 1) shallower convection with a lower maximum heating intensity; 2) a deeper moist layer, especially when the top of the moist layer extends within the cloud; and 3) enhanced vertical shear and higher latitude. The coexistence of several of the mechanisms listed here may produce explosivelike deepening of the cyclones. The shallow convection and Ekman layer dissipation slow down the wave propagation speed.

The model results not only confirm that the cumulus latent heat release is an essential ingredient to account for the rapid growth of the midlatitude cyclones, but also suggest the important indirect impacts of the strong sensible heat and moisture fluxes on the surface, as well as the importance of the enhanced vertical shear.

Acknowledgments. Our appreciation goes to Drs. I. Orlanski, Y. Hayashi and Y. Kurihara, whose comments helped to clarify the text. We are also grateful to Dr. Mak's comments on an earlier version of the manuscript. We thank Mrs. J. Callan for typing the manuscript. This work was supported, in part, by the Experimental Meteorology and Weather Modification Program for the Division of Atmospheric Sciences, National Science Foundation, under Grant ATM-8418624. We gratefully acknowledge such support.

APPENDIX A

Derivation of the Dispersion Equation (3.8) and Eigenfunction (3.10)

The right-hand side of (3.2) vanishes when $\eta(p) = 0$ outside the cloud. In terms of solutions $f_1(p)$ and $f_2(p)$, given by (3.6a, b), the eigenfunction can be expressed as

$$\Omega(p) = \begin{cases} B_1 f_1(p), & p_e \geq p > p_b \\ A(p)f_1(p) + B(p)f_2(p), & p_b \geq p \geq p_t \\ B_2 f_2(p), & p_t > p \geq p_u. \end{cases} \quad \text{(A1)}$$

By the method of variation of parameters we can write

$$A(p) = +Qk^2\Omega(p_m)\int^p \frac{\eta(t)f_2(t)}{tW_R(t)}\,dt + \tilde{A},$$

$$B(p) = -Qk^2\Omega(p_m)\int^p \frac{\eta(t)f_1(t)}{tW_R(t)}\,dt + \tilde{B}, \quad \text{(A2)}$$

where $\tilde{A}$ and $\tilde{B}$, as well as B_1, B_2 in (A.1), are constants to be determined. By use of the interfacial conditions (3.5a, b) we have

$$B(p_b) = 0, \quad \text{(A3a)}$$

$$A(p_t) = 0, \quad \text{(A3b)}$$

$$B_1 = A(p_b), \quad \text{(A3c)}$$

$$B_2 = B(p_t). \quad \text{(A3d)}$$

From (A3a) and (A3b), A, B are determined and

$$A(p) = \frac{Qk^2\Omega(p_m)}{f_1(p_u)}\int_{p_t}^{p} \frac{\eta(t)f_2(t)}{tW(t)}\,dt, \quad \text{(A4a)}$$

$$B(p) = -\frac{Qk^2\Omega(p_m)}{f_1(p_u)}\int_{p_b}^{p} \frac{\eta(t)f_1(t)}{tW(t)}\,dt. \quad \text{(A4b)}$$

From (A3c) and (A3d), we obtain

$$B_1 - \frac{Qk^2\Omega(p_m)}{f_1(p_u)}\int_{p_t}^{p_b} \frac{\eta(t)f_2(t)}{tW(t)}\,dt = 0, \quad \text{(A5)}$$

$$B_2 + \frac{Qk^2\Omega(p_m)}{f_1(p_u)}\int_{p_b}^{p_t} \frac{\eta(t)f_1(t)}{tW(t)}\,dt = 0. \quad \text{(A6)}$$

The expression for $\Omega(p_m)$ depends upon the value of p_m. We shall discuss two cases:

(i) $p_m \geq p_b$

In this case, the top of the moist convergence layer is located at or below the cloud base, and from (A1),

$$\Omega(p_m) = B_1 f_1(p_m).$$

(ii) $P_b > P_m > P_t$

When the top of the moist convergence layer is located within the cloud region, from (A1) it can be shown that

$$\Omega(p_m) = B_1 f_1(p_m)\Big/\left(1 - \frac{Qk^2}{f_1(p_u)}I\right), \quad \text{(A7)}$$

where

$$I = \int_{p_m}^{p_b} \frac{\eta(t)}{tW(t)}\,[f_1(t)f_2(p_m) - f_2(t)f_1(p_m)]dt.$$

In both cases, i.e., for p_m below or within the cloud, $\Omega(p_m)$ can always be expressed in terms of (A7), provided we define

$$I = \begin{cases} 0, & p_e \geq p_m \geq p_b \\ \displaystyle\int_{p_m}^{p_b} \frac{\eta(t)}{tW(t)}\,[f_1(t)f_2(p_m) - f_2(t)f_1(p_m)]dt, & \\ & p_b > p_m > p_t. \end{cases} \quad \text{(A8)}$$

Using (A7) in (A5), we obtain the dispersion relation

$$f_1(p_u) - Qk^2\left[I - f_1(p_m)\int_{p_t}^{p_b}\frac{\eta(t)f_2(t)}{tW(t)}\,dt\right] = 0; \quad \text{(A9)}$$

by using (A7) in (A6), we get

$$B_2 = B_1Qk^2\frac{f_1(p_m)}{f_1(p_u) - Qk^2I}\int_{p_t}^{p_b}\frac{\eta(t)f_1(t)}{tW(t)}\,dt, \quad \text{(A10)}$$

so that the eigenfunction (A1) is determined with an arbitrary multiplicative constant.

APPENDIX B

Expressions for $I_1(p)$ and $I_2(p)$

$$I_1(p) = -\frac{6\sqrt{2}}{\mu^3(p_b - p_t)^2}\{[k(1 - p_e - c)\Omega_2(p_e) - ir\Omega_2'(p_e)]\tilde{I}_1(p;\mu) - [k(1 - p_e - c)\Omega_1(p_e) - ir\Omega_1'(p_e)]\tilde{I}_2(p;\mu)\},$$

$$I_2(p) = -\frac{6\sqrt{2}}{\mu^3(p_b - p_t)^2}[\Omega_2(p_u)\tilde{I}_1(p;\mu) - \Omega_1(p_u)\tilde{I}_2(p;\mu)],$$

where

$$\tilde{I}_1(p;\mu) \equiv e^{-\mu(p+c-1)}\left[(2a-1)(p+c-1) + b_1 + \frac{b_0(p_b+c-1)(p_t+c-1)}{(p+c-1)(c-1)}\right] + b_2\{\ln(p+c-1) + F[-\mu(p+c-1)]\} + b_3[\ln p + F(-\mu p)],$$

$$b_0 = p_b + c - 1 - a(p_b + p_t + 2c - 2),$$

$$b_1 = b_0 - (2a-1)(p_b + p_t + c - 1) + \frac{2}{\mu}(2a-1),$$

$$b_2 = b_0\frac{1}{c-1}\left[p_b + p_t + 2c - 2 - \frac{(p_{b+c-1})(p_{t+c-1})}{(c-1)}\right] - (2a-1)\frac{(p_{b+c-1})(p_{t+c-1})}{(c-1)},$$

$$b_3 = e^{-\mu(c-1)}(\mu c - \mu + 1)[b_0 + (2a-1)(c-1)] \times\left\{1 - \frac{1}{c-1}\left[p_b + p_t + 2c - 2 - \frac{(p_b+c-1)(p_t+c-1)}{(c-1)}\right]\right\},$$

$$F(x) \equiv \sum_{n=1}^{\infty}\frac{x^n}{n\cdot n!},$$

$$\tilde{I}_2(p;\mu) \equiv -\tilde{I}_1(p;-\mu).$$

REFERENCES

Anthes, R. A., Y. H. Kuo and J. R. Gyakum, 1983: Numerical simulation of a case of explosive marine cyclogenesis. *Mon. Wea. Rev.*, **111**, 1174–1188.

Bosart, L. F., 1981: The presidents' day snowstorm of 18–19 February 1979: A subsynoptic-scale event. *Mon. Wea. Rev.*, **109**, 1542–1566.

Chang, C.-P., and R. T. Williams, 1974: On the shortwave cutoff of CISK. *J. Atmos. Sci.*, **31**, 830–833.

Charney, J. G., 1947: The dynamics of long waves in a baroclinic westerly current. *J. Meteor.*, **2**, 136–163.

Danard, M. B., and G. E. Ellenton, 1980: Physical influences on east coast cyclogenesis. *Atmos. Ocean*, **18**, 65–82.

Eady, E. T., 1949: Long waves and cyclone waves. *Tellus*, **1**, 33–52.

Gambo, K., 1976: The instability of medium-scale disturbances in a moist atmosphere. *J. Meteor. Soc. Japan.*, **54**, 191–207.

Gyakum, J. R., 1983a: On the evolution of the QEII storm. I: Synoptic aspects. *Mon. Wea. Rev.*, **111**, 1137–1155.

——, 1983b: On the evolution of the QEII storm. II: Dynamic and thermodynamic structure. *Mon. Wea. Rev.*, **111**, 1156–1173.

Hayashi, Y., 1970: A theory of large scale equatorial waves generated by condensation heat and accelerating the zonal wind. *J. Meteor. Soc. Japan*, **48**, 140–160.

Johnson, R. H., 1984: Partitioning tropical heat and moisture budgets into cumulus and mesoscale components for cumulus parameterization. *Mon. Wea. Rev.*, **112**, 1590–1601.

Kuo, H. L., 1965: On formation and intensification of tropical cyclones through latent heat release by cumulus convection. *J. Atmos. Sci.*, **22**, 40–63.

——, 1974: Further studies of the parameterization of the influences of cumulus convection on large scale flow. *J. Atmos. Sci.*, **31**, 1232–1240.

Mak, M. K., 1981: An inquiry on the nature of CISK. Part I. *Tellus*, **33**, 531–537.

——, 1982: On moist quasi-geostrophic baroclinic instability. *J. Atmos. Sci.*, **39**, 2028–2037.

——, 1983a: On moist quasi-geostrophic barotropic instability. *J. Atmos. Sci.*, **40**, 2349–2367.

——, 1983b: On moist quasi-geostrophic baroclinic instability in a general model. *Sci. Sin. (ser. B)*, **26**, 850–863.

Mullen, S. L., 1983: Explosive cyclogenesis associated with cyclones in polar air stream. *Mon. Wea. Rev.*, **111**, 1537–1552.

Rasmussen, E., 1979: The polar low as an extratropical CISK disturbance. *Quart. J. Roy. Meteor. Soc.*, **105**, 531–550.

Sanders, F., and J. R. Gyakum, 1980: Synoptic–dynamic climatology of the bomb. *Mon. Wea. Rev.*, **108**, 1589–1606.

Sardie, J. M., and T. T. Warner, 1983: On the mechanism for the development of polar lows. *J. Atmos. Sci.*, **40**, 869–881.

Smith, P. J., P. M. Dare and S. J. Lin, 1984: The impact of latent heat release on synoptic scale vertical motions and the development of an extratropical cyclone system. *Mon. Wea. Rev.*, **112**, 2421–2430.

Tracton, M. S., 1973: The role of cumulus convection in the development of extratropical cyclones. *Mon. Wea. Rev.*, **101**, 573–593.

Wang, B., A. Barcilon and L. N. Howard, 1985: On the dynamics of transient planetary waves. *J. Atmos. Sci.*, **42**, 1893–1910.